Sedimentology (1995) **42**, 453–471

A box model for non-entraining, suspension-driven gravity surges on horizontal surfaces

W. BRIAN DADE and HERBERT E. HUPPERT
Institute of Theoretical Geophysics, Department of Earth Sciences and Department of Applied Mathematics and Theoretical Physics, University of Cambridge, Cambridge CB2 3EQ, UK

ABSTRACT

The propagation of and the deposition from a turbulent gravity current generated by the release of a finite volume of a dense particle suspension is described by a box model. The approximate model consists of a set of simple equations, a predetermined, depth-dependent leading boundary condition and one experimentally determined parameter describing the trailing boundary condition. It yields predictions that agree well with existing laboratory observations and more complex theoretical models of non-eroding, non-entraining, suspension-driven flows on horizontal surfaces.

The essential features of gravity-surge behaviour have been observed and are captured accurately by the box model. These include the increased rate of downstream loss of flow momentum with increased particle setting velocity, the existence of maxima in the thickness of proximal deposits, and the downstream thinning of distal deposits. Our approximation for the final run-out distance, x_r, of a surge in deep water is given by $x_r \approx 3(g'_0 q_0^3 / w_s^2)^{1/5}$, where g'_0 is the initial reduced gravity of the surge, q_0 the initial two-dimensional volume, and w_s the average settling velocity of the particles in the suspension. A characteristic thickness of the resulting deposit is given by $\varphi_0 q_0 / x_r$, where φ_0 is the initial volumetric fraction of sediment suspended in the surge.

Our analysis provides additional insight into other features of gravity-surge dynamics and deposits, including the potential for the thickening of currents with time, the maintenance of inertial conditions and the potential for strong feedback in the sorting of particle sizes in the downstream direction at travel distances approaching x_r. Box-model approximations for the evolution of gravity surges thus provide a useful starting point for analyses of some naturally occurring turbidity surges and their deposits.

INTRODUCTION

A gravity current occurs whenever a density difference between two fluids gives rise to the lateral flow of one fluid into the other. The term gravity surge applies specifically to the density driven flow of a fluid with finite volume. Turbidity currents are examples of geologically important gravity surges in which the excess density is derived from the presence of particles dispersed throughout the flow and in which the particles are suspended within the current by turbulence generated by the flow. Suspension-driven gravity surges ultimately dissipate due to the damping of turbulence by viscous friction or internal density stratification, and due to the loss of excess density through entrainment of ambient fluid or deposition of suspended particles.

The propagation of and the deposition from these complicated flows pose challenging problems for geologists and engineers interested in sedimentation on continental margins. Turbidity surges in ancient seas have contributed to the formation of some petroleum reservoirs, for

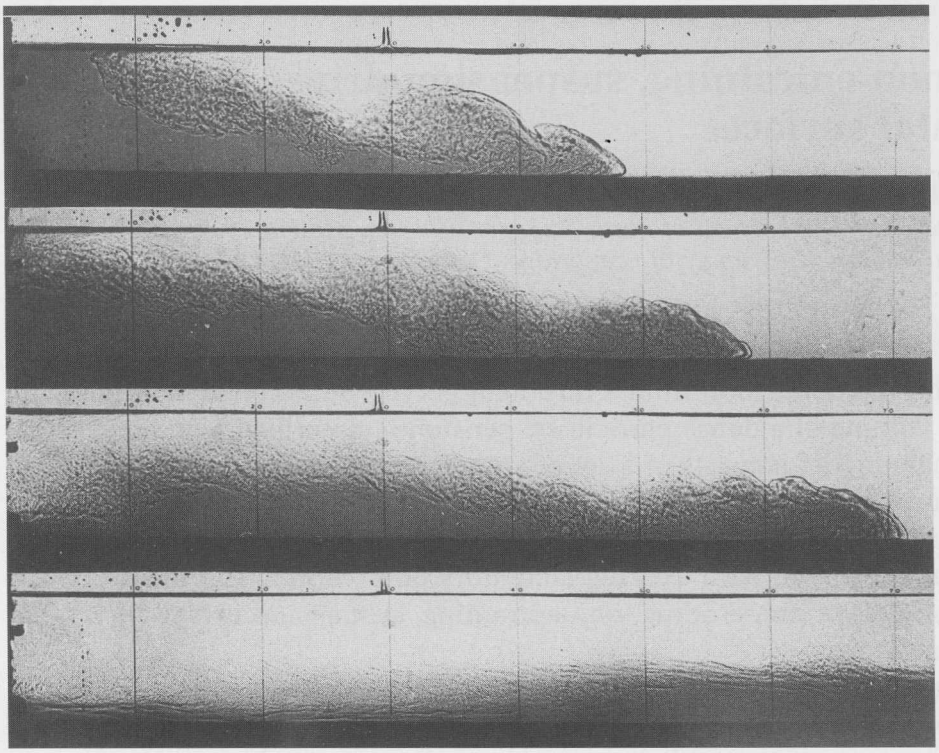

Fig. 1. (a)

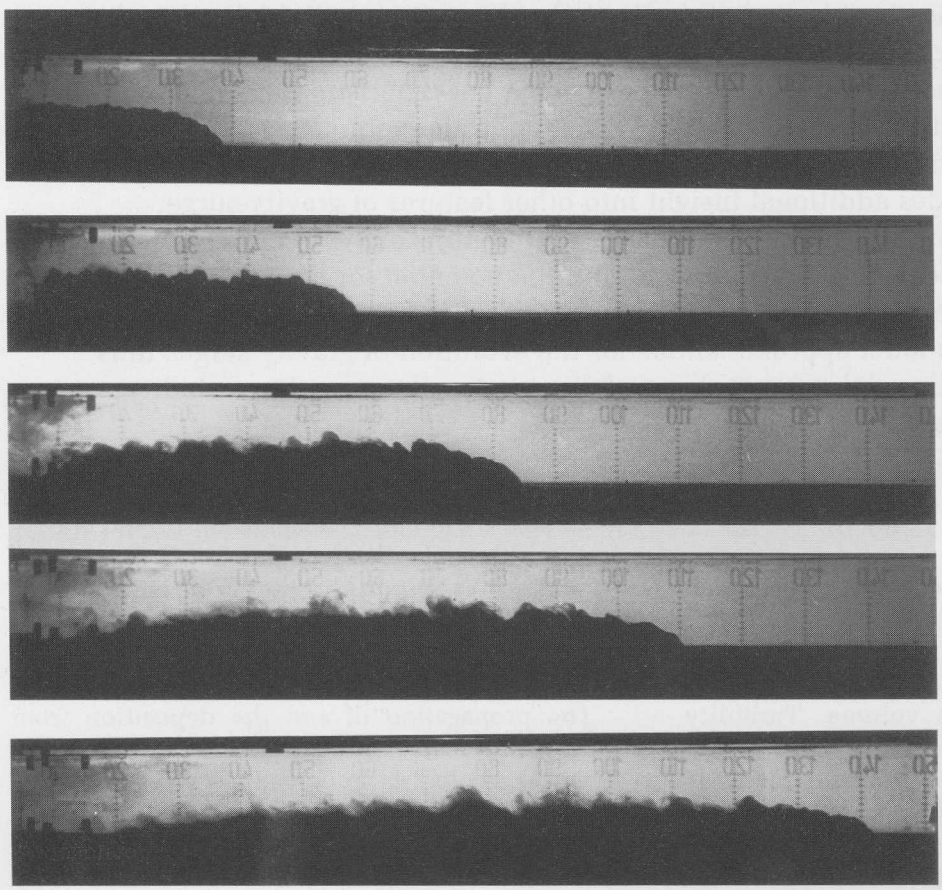

Fig. 1. (b)

example, and modern turbidity surges may interfere with offshore structures designed to tap those same petroleum resources. Our work is motivated by a desire to understand suspension-driven gravity surges and represents an extention of many studies that have appeared in the geological literature during the last few decades (e.g. Middleton 1966a,b, 1967; Riddell, 1969; Middleton & Neal, 1989).

Bonnecaze *et al.* (1993), hereafter denoted by BHL, are among the most recent to analyse the behaviour of two-dimensional gravity surges undergoing dissipation due to particle deposition. They solved numerically the coupled equations that describe the conservation of mass and momentum to obtain predictions of the motion of a suspension-driven gravity flow as it propagates across a horizontal surface. Their approach incorporates no freely adjustable parameters, yet yields predictions that compare well with their experimental observations on the rate of advance of a deposit-forming surge and the distribution of the deposits. Their theory also indicates that a constant-volume, suspension-driven gravity current evolves from a self-similar regime of collapse that is characteristic of a compositionally driven (e.g. saline) surge into a bore-like flow. Differences in thickness along the length of a gravity surge during early stages of its evolution accompany spatial variation in excess density due to particle settling. A relatively greater rate of density loss in the current tail reduces the rearward pressure gradient that would otherwise inhibit forward fluid motion in that region. Accumulation of rearward fluid behind the slower moving current-head ensues, and a dense, bore-like cloud of suspended particles develops in time.

Bonnecaze *et al.* (1993) also found that for an accurate description of their experimental observations a two-layer model had to be considered to accommodate the behaviour of the gravity surge in shallow-water surroundings. Specifically, a shallow-water gravity current interacts with the confined counterflow of the fluid into which it is issuing. As a consequence the intruding gravity surge exhibits a boundary condition at the moving front which is dependent on the ratio of current thickness to the ambient depth. This behaviour characterizes a slumping phase observed in the early development of many laboratory gravity currents (Huppert & Simpson, 1980).

Simplifications made by BHL to obtain their theoretical results include the explicit assumptions that both momentum and mass of the inviscid, Boussinesq current are distributed uniformly in the vertical and that both entrainment of ambient fluid and frictional effects are negligible. Even with these simplifications, however, the numerical solution of the equations describing particle-driven gravity surges becomes unwieldy for many geological applications.

We present here straightforward analytical expressions that describe the evolution of the simplest of slumping, suspension-driven gravity currents as they intrude into deep or shallow water. Our approach can be thought of as an extension to the box model of Huppert & Simpson (1980), which incorporates the relatively slow settling of particles uniformly suspended in the turbulent flow. Evolution of the two-dimensional, inertial current is then considered to occur through a series of rectangles of constant area and uniform composition. The attendant assumption of uniform depth along the length of the flow at any instant in time is a reasonable one, as is shown in Fig. 1 for a 'base-case' saline gravity surge and an analogous suspension-driven current. It is for a box-model approach, moreover, that the empirical moving-front boundary condition used by BHL, and which we again use here, was originally confirmed.

We provide an analysis for both deep-water and shallow-water conditions, and focus on the comparison between our model predictions and existing observations of slumping gravity surges generated in the laboratory. Good agreement between our predictions and the experimental observations leads us to several important interpretations of suspension-current behaviour. Among these points of interest, our results are consistent with the conclusion reached by

Fig. 1. (a) Shadowgraphs at approximately 4·4, 6·8, 9·7 and 17·5 s after release of a two-dimensional, saline gravity current with h_0=10 cm, l_0=30 cm, and g'_0=11 cm s^{-2}. The thin vertical lines are at 10 cm intervals and the end wall can just be seen on the far left. The gravity current is in the slumping phase in each view. In the first image, the return flow of the lighter, undyed fluid has not yet reached the trailing wall and the thickness of the intruding gravity current is variable over its length. In the second view, the current shape is tending towards uniform thickness. It is clearly box-like in the third and fourth views. Note the thin tail extending toward the trailing wall in the last shadowgraph. (From Huppert & Simpson, 1980, Fig. 9, plate 1.) (b) Suspension-driven gravity current analogous to that shown in (a).

Hallworth *et al.* (1993) that slumping gravity currents entrain a little or no ambient fluid. We also reaffirm the notion introduced by BHL that suspension currents generated in the laboratory may propagate in the slumping regime for relatively longer periods of time than do analogous saline currents. Laboratory gravity currents are used frequently as analogues for flows of environmental interest, and the analytical expressions presented here are simpler to apply to either laboratory data or field observations than the complete numerical solution of BHL. In one application, for example, we show that predictions from our model are in good agreement with the experimental observations of Middleton & Neal (1989) regarding the scaling relationships between the characteristic parameters of a surge and its deposit. The box-model approach also provides new insights regarding the evolution of suspension-driven gravity flows that may be extended to the analysis of some deposits generated by natural phenomenon. In another paper, we explore the model behaviour of a fully developed, fluid-entraining turbidity surge on a slope (Dade *et al.*, 1994).

The literature on the underlying anlaysis of inertial, compositionally driven currents is discussed briefly by BHL. More detailed discussions of the broad range of gravity-current behaviour are available in Simpson (1982, 1987), and a review of geological aspects of these flows appears in Allen (1984). A recent summary of experimental studies designed to examine the behaviour of suspension–driven currents appears in Middleton (1993).

In the next section of our paper we describe our box-model approximations for suspension-driven gravity surges. The description presents the mathematical development and discusses the results of our analysis. This exposition is followed by a comparison between the model predictions and the experimental observations reported by BHL. In that section we discuss the graphical representations of our analytical results and show that these are in good agreement with the experimental data. We then consider the effects of more than one grain size on the behaviour of a suspension-driven surge. In the final section, we discuss additional ramifications for the behaviour of these complicated flows both in the laboratory and in the field. In particular, we demonstrate that the simple scalings which emerge from our analysis may be used to reconstruct past events in which turbidities were deposited on elongate basin plains.

BOX-MODEL APPROXIMATIONS

The following analysis is based on the assumption that a two-dimensional gravity current is an inviscid, Boussinesq flow which results from the release of an initially stationary volume of dense fluid into less dense surroundings. We make several additional, simplifying assumptions. Many of the expressions presented below are thus approximations only and the $\approx$ sign is used throughout our analysis to differentiate between these and exact relations.

As in Huppert & Simpson (1980), gravity-surge collapse and subsequent motion across a horizontal surface is understood to be controlled primarily by the pressure gradient existing at the current head. A steady-state balance there then gives rise to the relationship

$$u_N = Fr_N(g'h)^{1/2}, \tag{1}$$

where u_N is the velocity of the current head, Fr_N the Froude number at the current head, and h the current thickness. In Eq. (1), g', the reduced gravity of currents with density ρ_c propagating into a fluid of ambient density ρ_a, is given by

$$g' = g(\rho_c - \rho_a)/\rho_a, \tag{2a}$$

where g is the acceleration due to gravity, and

$$\rho_c = (\rho_p - \rho_a)\varphi + \rho_a, \tag{2b}$$

where ρ_p and φ are the density and volumetric fraction of the particles, respectively. Note that g' is linearly dependent on φ, the volumetric fraction of particles, and is thus a function of time in gravity currents subject to the loss of excess density through the settling of suspended particles. Recognition that the temporal evolution of g' is very slow relative to the time-scale of the propagation of a surge provides the basis for our small-perturbation approach to the existing box model for compositionally driven flows. As we show, this assumption facilitates the decoupling of the equations that describe the conservation of momentum and particulate mass, and leads to the approximations made below.

To describe the depth dependence of the leading boundary condition of Eq. (1) for slumping gravity currents, Huppert & Simpson (1980) found experimentally that

$$Fr_N = 1/2(h/d)^{-1/3} \qquad 0{\cdot}075 \leq h/d < 1 \tag{3a}$$

and

$$Fr_N = 1{\cdot}19 \qquad h/d < 0{\cdot}075, \tag{3b}$$

where d is the depth of the ambient surroundings.

This boundary condition at the moving front implicitly incorporates the effects of friction and any small entrainment of ambient fluid.

We assume further that a volume-conserving, two-dimensional current evolves through a series of equal-area rectangles such that

$$q_0 = h_0 l_0 = h(x_N - x_T), \tag{4}$$

where h_0 and l_0 are the initial thickness and length of the surge, and x_N and x_T represent the positions of the leading and trailing boundaries of the turbulent current as it propagates downstream.

Gravity-surge intrusion into deep-water surroundings

We begin by considering a flow for which the thickness h is always less than $0{\cdot}075d$, the concentration φ is conserved and the position of the current tail remains fixed at the origin. Then substitution of $u_N = dx_N/dt$ into Eq. (1) and integration of the result using Eqs (3b) and (4) with $x_T = 0$ yields a relationship between height h and time t for times greater than the characteristic time-scale $(h_0/g')^{1/2}$. This relationship is given by

$$h = 0{\cdot}68(q_0^2/g')^{1/3} t^{-2/3} \tag{5a}$$

and corresponds to the self-similar form for the height of a compositionally driven surge. The leading coefficient in Eq. (5a) is related to the constant Froude number defined in Eq. (3b).

To investigate the evolution of a sediment-laden, deposit-forming gravity current, we allow for the slow variation of g' and the possibility that $x_T \neq 0$ by substituting Eq. (2) into Eq. (5a) to obtain

$$h \approx 0{\cdot}68 c_d (q_0^2/g_0')^{1/3} (\varphi/\varphi_0)^{-1/3} t^{-2/3}, \tag{5b}$$

where g_0' is the initial value of g'. The newly introduced coefficient c_d is slowly varying and incorporates the histories of both the particle concentration and the motion of the current tail, as is shown in Appendix A. In the following developments, however, we treat c_d as a constant. It will vary between currents but, in general, is close to unity, which is the exact value expected for compositionally driven flows. This coefficient can be considered as a temporally averaged shape factor for the evolving current.

This approximation is used to analyse the slow loss of particulate mass as follows. Particle concentration is assumed to be distributed uniformly throughout the gravity surge, and its conservation is described by the settling law for a dilute, non-eroding, turbulent suspension (e.g. Martin & Nokes 1988). The rate of change of total particulate volume $q_0\varphi$ is then given by the loss due to settling over the length of the current.

$$\frac{d(q_0\varphi)}{dt} = -w_s\varphi(x_N - x_T), \tag{6a}$$

where w_s is the still-water settling velocity of the fine particles in dilute aqueous suspension and is proportional to the square of the particle diameter for particle sizes corresponding to fine quartz sand or smaller. The settling law defined in Eq. (6a) requires that w_s be very small relative to the characteristic velocity of the gravity current and is consistent with the notion that the gravity current is slowly varying in general. Total volume is conserved in non-entraining flows and Eq. (6a) can be reduced to

$$\frac{d\varphi}{dt} = -\frac{w_s\varphi}{h}. \tag{6b}$$

Substitution of Eq. (5b) into Eq. (6b) and rendering the results dimensionless with respect to the length-scale h_0, the time-scale $(h_0/g_0')^{1/2}$ and the initial concentration φ_0, yields

$$\frac{d\Phi}{dT} \approx -\frac{\beta}{0{\cdot}68\, c_d Q_0^{2/3}} \Phi^{4/3} T^{2/3}, \tag{7}$$

where the upper-case symbols represent the dimensionless forms of their lower-case equivalents. The new parameter β introduced in Eq. (7) is defined by

$$\beta = w_s/(g_0' h_0)^{1/2}, \tag{8}$$

and represents the particle settling velocity made dimensionless with respect to the characteristic velocity of the gravity current. Variable β is assumed always to be much less than unity for fine particles in a well-mixed turbulent suspension.

Equation 7 has the solution for the initial condition $\varphi = \varphi_0$ (i.e. $\Phi = 1$ at $T = 0$) given by

$$\Phi \approx \left(1 + \frac{\beta}{3{\cdot}4\, c_d Q_0^{2/3}} T^{5/3}\right)^{-3}. \tag{9}$$

The term in parentheses on the right-hand side of Eq. (9) embodies the effects of the slow settling of the particles from the driving suspension. For convenience we abbreviate this term to Ψ_d given by

$$\Psi_d = 1 + (\sigma_d T)^{5/3}, \tag{10a}$$

where

$$\sigma_d = \left(\frac{\beta}{3{\cdot}4\, c_d Q_0^{2/3}}\right)^{3/5}. \tag{10b}$$

Note that Ψ_d is a function of time, though by assumption σ_d is not. The dimensionless concentration of particles is then given by $\Phi \approx \Psi_d^{-3}$, and the effects of particle settling on the dynamics of the surge become significant as dimensionless time approaches and exceeds σ_d^{-1}. In dimensional terms, this corresponds to a characteristic time-scale proportional to $(q_0^2/g_0' w_s^3)^{1/5}$ on which the effects of particle settling become important.

We now retrace our steps and correct current height h and travel distance x_N to include the newly defined effects of a slowly evolving particle concentration. Substituting Eqs (9) and (10) into Eq. (5b), we find that for dimensionless time $T>1$ the dimensionless thickness of the surge is given approximately by

$$H \approx 0{\cdot}68\, c_d Q_0^{2/3} \Psi_d T^{-2/3}. \tag{11}$$

Substitution of Eqs (2), (9), (10) and (11) into Eq. (1) and non-dimensionalizing yields an estimate of the dimensionless velocity of the surge front given by

$$U_N \approx 0{\cdot}98 c_d^{1/2} Q_0^{1/3} \Psi_d^{-1} T^{-1/3}. \tag{12}$$

Note that U_N diminishes as T^{-2} for large T, which indicates that integration of Eq. (12) with respect to time in order to determine the frontal travel distance $X_N = x_N/h_0$ will result in a finite asymptotic limit.

Explicit integration of Eq. (12) to obtain estimates of the travel distance of the surge head as a function of time is accomplished with the help of comprehensive tables (e.g. Gradshteyn & Ryzhik, 1980) or mathematics packages for the desk-top computer (e.g. Mathematica™). In dimensionless terms the propagation distance X_N of the suspension-driven surge is given by

$$X_N \approx (Q_0/\sigma_d^2)^{1/3}\, f_d(\sigma_d T), \tag{13}$$

where the origin is taken at the leading edge upon release and $f_d(\sigma_d T)$ is given in Appendix B. The position of the tail X_T, which is one surge length behind the advancing front, can be calculated from this expression and from the relationship $X_T = X_N - Q_0/H$ (cf. Eq. 4).

As σ_d tends to zero, corresponding to a buoyancy-conserving density current, c_d tends to 1 and Eq. (13) can be shown by a series expansion of $f_d(T_d T)$ to be equivalent to the expression for a compositionally driven current, $X_N = 1{\cdot}47 Q_0 T^{2/3}$ (which is consistent with the representation in Eq. (A4) in Appendix A). On the other hand, as $\sigma_d T$ becomes very large, Eq. (13) can be shown to have the asymptotic limit

$$X_r \approx 3{\cdot}17\, c_d^{9/10} \beta^{-2/5} Q_0^{3/5} \qquad (\sigma_d T \gg 1) \tag{14a}$$

for the dimensionless travel distance X_N of a deep-water surge. This result corresponds to the dimensional limit

$$x_r \approx 3{\cdot}17\, c_d^{9/10} (g_0' q_0^3/w_s^2)^{1/5} \tag{14b}$$

at times sufficiently large that

$$t \gg 2{\cdot}1\, c_d^{3/5} (q_0^2/g_0' w_s^3)^{1/5}. \tag{14c}$$

In reality, a surge does not come to an absolute halt. This result is rather a consequence of the approximations used in the derivative of Eq. 13. The distance x_r defined in Eq. (14b) nevertheless provides the scale of the run-out distance of a non-entraining, deep-water surge. This length-scale essentially corresponds to the distance beyond which the propagation speed of the surge vanishes due to the significant loss of driving buoyancy through deposition. Note that it differs from the value determined by Dade *et al.* (1994) for a deep-water current that travels down a uniform slope and entrains ambient fluid. For fine particles in the Stokes' settling regime, Eq. (14b) indicates that the overall run-out distance x_r achieved by a suspension-driven surge on a horizontal surface is proportional to $\varphi_0^{1/5}$, $d_p^{-4/5}$, $h_0^{3/5}$ and $l_0^{3/5}$, where d_p is the particle diameter.

Gravity-current intrusion into shallow-water surroundings

We begin again by considering a flow for which the thickness h of a surge is always greater than $0{\cdot}075d$, but as before the concentration is conserved and the position of the current tail remains fixed at the origin. Then proceeding as before, except using Eq. (3a) rather than (3b), we find that

$$h \approx 1{\cdot}59\, (q_0^6/g'^3 d^2)^{1/7}\, t^{-6/7} \tag{15a}$$

for times greater than the characteristic time-scale $(h_0/g')^{1/2}$.

As in the case of deep-water flows, we allow approximately for the slow variation of g' and the possibility that $x_T \neq 0$ in suspension-driven currents by substituting Eq. (2) into Eq. (15a) to obtain

$$h \approx 1{\cdot}59\, c_s (q_0^6/g_0'^3 d^2)^{1/7}\, (\varphi/\varphi_0)^{-3/7}\, t^{-6/7}. \tag{15b}$$

The coefficient c_s is analogous to c_d introduced in Eq. (5b). It is slowly varying and incorporates the histories of both the particle concentration and the motion of the current tail, as is shown in Appendix A. As in our analysis for deep-water flows we treat c_s as a constant which may vary

between currents but in general is close to unity, the value expected for compositionally driven flows.

By analogy with the earlier analysis for deep-water gravity surges, substitution of Eq. (15b) into Eq. (6) and solving the resulting expression to match the initial condition $\varphi=\varphi_0$ yields, in dimensionless terms,

$$\Phi \approx \left(1+\frac{D^{2/7}\beta}{6{\cdot}9\ c_s Q_0^{6/7}}\ T^{13/7}\right)^{-7/3}, \tag{16}$$

where $D=d/h_0$. The term in parentheses on the right-hand side of Eq. (16) embodies the effects of the slow settling of particles in a shallow-water flow. For convenience we abbreviate this term to Ψ_s given by

$$\Psi_s = 1+(\sigma_s T)^{13/7} \tag{17a}$$

where

$$\sigma_s = \left(\frac{D^{2/7}\beta}{6{\cdot}9\ c_s Q_0^{6/7}}\right)^{7/13}. \tag{17b}$$

Thus $\Phi \approx \Psi_s^{-7/3}$ for suspension-driven surges in shallow-water surroundings and the effects of particle settling become significant at dimensionless time approaching and exceeding σ_s^{-1}. In dimensional terms, this corresponds to a characteristic time-scale $(q_0^6/h_0^2 g_0'^3 w_s^7)^{1/13}$ on which the effects of particle settling become important. This scaling is different from that found for deep-water flows.

Again we retrace our steps through the original approximations for the dimensionless thickness H and frontal velocity U_N of the gravity surge, correcting for the slow evolution of excess density due to particle settling. Substituting Eqs (16) and (17) into Eq. (15b), we find that

$$H \approx 1{\cdot}59\ c_s D^{-2/7} Q_0^{6/7} \Psi_s T^{-6/7}. \tag{18}$$

With this result and Eqs (1) and (3a) we then find that

$$\begin{aligned} U_N &= 1/2 D^{1/3} H^{1/6} \Phi^{1/2} \\ &\approx 0{\cdot}54\ c_s^{1/6} (Q_0 D^2)^{1/7} \Psi_s^{-1} T^{-1/7}, \end{aligned} \tag{19}$$

from which we see that the integrated quantity X_N will be finite because U_N diminishes as T^{-2} for large T.

Again with the help of mathematical software packages, integration of this last result with respect to time yields an approximation for the dimensionless distance of travel of the surge front, which is given by

$$X_N \approx (Q_0 D^2/\sigma_s^6)^{1/7}\ f_s(\sigma_s T), \tag{20}$$

where the origin is at the leading edge of the current upon release and $f_s(\sigma_s T)$ is given in Appendix B.

As the product $\sigma_s T$ becomes infinitely large, X_N for a surge in shallow water approaches the asymptotic limit given by

$$X_r \approx 2{\cdot}24\ c_s^{49/78} D^{2/13} \beta^{-6/13} Q_0^{7/13} \qquad (\sigma_s T \gg 1). \tag{21a}$$

This result yields a dimensional estimate for the run-out distance of the surge given by

$$x_r \approx 2{\cdot}24\ c_s^{49/78} D^{2/13} (g_0'^3 q_0^7 h_0^2 / w_s^6)^{1/13} \tag{21b}$$

at times sufficiently large that

$$t \gg 2{\cdot}8\ c_s^{7/13} D^{-2/13} (g_0^6/h_0^2 g_0'^3 w_s^7)^{1/13}. \tag{21c}$$

If the driving suspension comprises fine particles in the Stokes settling regime and D is held constant, Eq. (21b) indicates that the overall length of run-out of shallow-water surges and their corresponding deposits are proportional to $\varphi_0^{3/13}$, $d_p^{-12/13}$, $h_0^{-9/13}$ and $l_0^{7/13}$. These scalings are different from those found for a deep-water surge (cf. Eq. 14).

Gravity currents exhibiting a transition between slumping and deep-water behaviour can be described by matching Eq. (12) to Eq. (19) at the time at which h equals $0{\cdot}075d$, and integrating forward from that instant.

Distribution of particle deposits

At any point on the bed along the current's path of travel, deposition is related to the instanteneous rate of loss of the total particulate mass per unit length of the surge, $-(x_N-x_T)^{-1}\ \mathrm{d}(q_0\varphi)/\mathrm{d}t$. The accumulation of sediment at the point of interest can be estimated from the total loss of particle mass during the approximate time of passage $(x_N-x_T)/u_m$ of the current across that location, where $u_m=\mathrm{d}x_m/\mathrm{d}t$ is the propagation speed of the mid-point of the surge at a distance $x_m=(x_N+x_T)/2$ from the origin. Thus deposition is described by a gradient in the particle concentration field, $-(u_m)^{-1}\ \mathrm{d}(q_0\varphi)/\mathrm{d}t = -\mathrm{d}(q_0\varphi)/\mathrm{d}x_m$. In order to calculate deposition at a point along the path of travel, we need to estimate the propagation speed u_m.

To obtain this estimate, we note that $u_m=(1/2)(\mathrm{d}x_N/\mathrm{d}t+\mathrm{d}x_T/\mathrm{d}t)$. Using this formulation in dimensionless terms, the propagation speed U_m of the surge mid-point X_m is given, for a deep-water flow, by

$$U_m = \mathrm{d}X_m/\mathrm{d}T \approx \chi_d U_N, \tag{22a}$$

where

$$\chi_d = [(c_d^{3/2} + 0{\cdot}75)\Psi_d - 1{\cdot}25]/(c_d^{3/2}\Psi_d) \quad (22b)$$

and the composition of χ_d reflects the terms obtained in deriving dx_N/dt and dx_T/dt. In the case of a suspension current in shallow-water surroundings, on the other hand, the propagation speed U_m of the centre of gravity of the surge is given by

$$U_m \approx \chi_s U_N, \quad (23a)$$

where

$$\chi_s = [(c_s^{7/6} + 0{\cdot}58)\Psi_s - 1{\cdot}08]/(c_s^{7/6}\Psi_s). \quad (23b)$$

Both χ_d and χ_s are weak functions of time. Equations (22) and (23) indicate correctly that in the initial stages of a flow accelerating from rest, the tail of the surge remains stationary at the origin, $\Psi_d \approx \Psi_s \approx 1$ and $c_d \approx c_s \approx 1$ and thus $U_m/U_N \approx 1/2$. At large times, however, the tail has moved from the origin and the behaviours of χ_d and χ_s are such that U_m/U_N exceeds unity. This result reflects the tendency of the body to move faster than, and to supply material to, the head of the current.

Multiplying the right-hand side of Eq. (6a) by u_m^{-1} yields a direct estimate of the deposit density δ (mass per unit of bed area),

$$\delta = \rho_p w_s q_0 \varphi/(u_m h), \quad (24a)$$

evaluated at the mid-point of the gravity surge $x_m = (x_N + x_T)/2$. Expressions for u_m defined in Eqs (22) or (23) and expressions for particle concentration φ and height h can be substituted into Eq. (6a) and rearranged to yield the divergence of the particulate mass during the time of passage of a surge.

Equation (24a) can be expressed in dimensionless terms as

$$\eta \equiv \frac{\delta}{\rho_p \varphi_0 h_0} \approx \beta Q_0 \Phi/(U_m H) \quad (24b)$$

and is evaluated at $X_m = X_N - Q_0/(2h)$. A characteristic density of the deposit can be calculated then in dimensionless terms as

$$\hat{\eta} \approx Q_0/X_r \approx 0{\cdot}32 c_d^{-9/10}\beta^{2/5}Q_0^{2/5}. \quad (25)$$

Substitution of Eqs (9–12) and (22a) into Eq. (24b), on the other hand, yields

$$\eta \approx 1{\cdot}5(c_d^{3/2}\chi_d)^{-1}\beta T \Psi_d^{-3} \quad (26)$$

as the dimensionless density of deposit η for a surge in deep water as a function of dimensionless time T. This expression is zero at $T=0$, rises to a maximum and then decays algebraically to zero as T tends to infinity.

The density (or thickness) of a surge deposit is maximal in time when

$$d\eta/dT = 0. \quad (27)$$

The solution to this condition when applied to Eq. (26) with c_d assumed to be unity provides an estimate of the maximal density of deposit η_{max} in deep-water surroundings of

$$\eta_{max} \approx \beta^{2/5}Q_0^{2/5} \approx 3\hat{\eta}. \quad (28a)$$

This is laid down at the dimensionless travel time T_{max} given by

$$T_{max} \approx 0{\cdot}66\beta^{-3/5}Q_0^{2/5}, \quad (28b)$$

or at a dimensionless distance to the surge mid-point given by

$$X_{max} \approx 0{\cdot}59\beta^{-2/5}Q_0^{3/5}, \quad (28c)$$

Equations (25) and (28a) can be re-expressed in dimensional terms to give a characteristic thickness $\hat{\tau} \approx 1/3 c_d^{-9/10}(\varphi_0/\varphi_b)(w_s^2 q_0^2/g_0')^{1/5}$ and maximal thickness $3\hat{\tau}$ of the deposit, where φ_b is the volumetric fraction of solids in the bed, which typically takes a value of about 0·5. For fine particles in the Stokes' settling regime, we note that both the characteristic and maximal thickness of a deposit generated by a deep-water surge must thus scale with $\varphi_0^{4/5}$, $d_p^{4/5}$, $h_0^{2/5}$, and $l_0^{2/5}$. From Eq. (28c) moreover, we find that the maximum thickness occurs at a distance $x_{max} \approx 0{\cdot}59(g_0' q_0^3/w_s^2)^{1/5}$ from the source. Comparing this result with our estimate given in Eq. (14b) for the run-out distance of a deep-water surge for which $c_d = 1$, we note that $x_{max}/x_r = 0{\cdot}59/3{\cdot}17 \approx 1/5$. The deep-water surge deposit is thus lenticular in shape as viewed in longitudinal section and exhibits a maximal thickness that is about three times the average thickness and at a distance downstream from the origin of the deposit-forming flow that is about one-fifth of the overal length of the deposit.

In the case of a surge in shallow-water surroundings, a characteristic density of deposit generated by a surge in shallow water is given by

$$\hat{\eta} \approx Q_0/X_r \approx 0{\cdot}45 c_s^{-49/78}\beta^{6/13}D^{-2/13}Q_0^{6/13}. \quad (29)$$

Substitution of Eqs (16–29) and (23) into Eq. (24b) yields an estimate of the dimensionless density of deposit η as a function of time given by

$$\eta \approx 1{\cdot}2(c_s^{7/6}\chi_s)^{-1}\beta T \Psi_s^{-7/3}. \quad (30)$$

As for the expression for a deposit generated by a deep-water current, Eq. (30) is zero at $T=0$, rises to a maximum and then decays algebraically to zero as T tends to infinity. The solution to the condition described by Eq. (27) when applied to

Eq. (29) with c_s assumed to be unity provides an estimate of the maximal density or thickness of the deposit given by

$$\eta_{max} \approx 1{\cdot}34\beta^{6/13}D^{-2/13}Q_0^{6/13} \approx 3\hat{\eta}. \quad (31a)$$

This maximum is laid down at a dimensionless time given by

$$T_{max} \approx 1{\cdot}08\beta^{-7/13}D^{-2/13}Q_0^{6/13} \quad (31b)$$

or at a dimensionless distance given by

$$X_{max} \approx 0{\cdot}35\beta^{-6/13}D^{-2/13}Q_0^{7/13}. \quad (31c)$$

Equations (30) and (31a) can be re-expressed in dimensional terms to give a characteristic deposit thickness $\hat{\tau} \approx 0{\cdot}45D^{-2/13}(\varphi_0/\varphi_b)(w_s^6 q_0^6/g_0'^3 h_0^2)^{1/13}$ and the maximal deposit thickness $3 \times \hat{\tau}$ generated by shallow-water surges. For fine particles in the Stokes' settling regime and for shallow-water conditions in which the surge height is initially equal to the channel depth (D=1), both the characteristic and maximal thickness of a deposit generated by a shallow-water surge is proportional to $\varphi_0^{10/13}$, $d_p^{12/13}$, $h_0^{4/13}$, and $l_0^{6/13}$. Thus deposits generated by shallow-water flows exhibit power-law relationships that are similar, but not identical, to the deep-water scalings given above.

Middleton & Neal (1989) found experimentally that the characteristic thickness of surge deposits generated by various suspension-driven surges in a horizontal channel with D=1 was proportional to $\varphi_0^{0{\cdot}7}$, d_p, $h_0^{0{\cdot}4}$, and $l_0^{0{\cdot}5}$. Our predictions of the shallow-water scalings that relate deposit thickness and surge properties as given above are very close to these empirical results. As an interesting aside, our predictions for the characteristic thickness of a deposit generated by a shallow-water surge with D=1 can also be shown to scale as

$$\hat{\tau}^2/q_0 \approx [(1/2)^{12/13}(\varphi_0/\varphi_b)^2(h_0^2/q_0)^{1/13}](w_s/u_0)^{12/13},$$

where $u_0 = 1/2(g_0'h_0)^{1/2}$ is the velocity scale for the flow at the instant of release, as given by Eq. (3a). This form is virtually identical to the empirical one reported by Middleton & Neal (cf. eq. (7) in their text), and reveals the dependence of the multiplicative coefficient in their result on the quantities in brackets: the shallow-water Froude number at the instant of surge release (=1/2), the solids concentration in the initial suspension and in the bed, and the lock geometry.

The maximum in the density or thickness of a deposit generated by a shallow-water surge occurs at a distance from the source given from Eq. (31c) as $x_{max} \approx 0{\cdot}35D^{-2/13}(g_0'^3 q_0^7 h_0^2/w_s^6)^{1/13}$. Comparing this result with our estimate for the run-out distance x_r given in Eq. (21b), we note that $x_{max}/x_r = 0{\cdot}35/2{\cdot}24$, or about 1/6. Thus deposits generated by shallow-water surges are similar in gross morphology to, but slightly more elongate than, their deep-water counterparts.

Maxima in the density (or thickness) of surge deposits result from two competing factors in the temporally evolving current. These are the diminishing rates of deposition and surge speed at a fixed point along the travel path. At early times, the rapidly moving body of the turbulent current passes over a point very quickly and so little mass is laid down despite high rates of deposition. During these early times the current is thinning rapidly and the local deposition rate is thus increasing dramatically. At large times, duration of passage of the surge over a fixed point is much longer, but the slowly moving current has relatively little to deposit. For a gravity current driven by a monodisperse suspension, Eqs (28c) and (31c) suggest that downstream displacement of the maxima in densities of the resulting deposits increases with increasing initial aspect ratio $Q_0 = l_0/h_0$ and diminishing dimensionless particle settling velocity β. In the case of shallow-water gravity currents, downstream distribution of deposits is weakly dependent on the relative ambient depth $D = d/h_0$.

The precise descriptions of the propagation of a surge and the distribution of the resulting particle deposit are clearly dependent on the experimentally determined coefficients c_d or c_s that were introduced to accommodate the unknown trailing boundary conditions of the current. Comparison of our box-model approximations with experimental observations of both propagation rates and deposits of particle-driven currents is thus important for the verification of this approach.

COMPARISON OF BOX-MODEL APPROXIMATIONS AND EXPERIMENT

Bonnecaze *et al.* (1993) performed several experiments with suspension-driven gravity currents in order to validate their numerical model. Both travel distance as a function of time and areal density of deposits were determined for a range of parameters. Their experiments were conducted in a large glass tank (10 m long by 0·26 m wide by 0·48 m high) which was filled with tap water to a depth of 0·30 m. The volume of the lock holding the initial suspension at rest was $1{\cdot}17 \times 10^{-2}$ m^3, with D=1 and Q_0=0·5. The suspended particles providing excess density were silicon carbide (density 3217 kg m^{-3}), with different particle

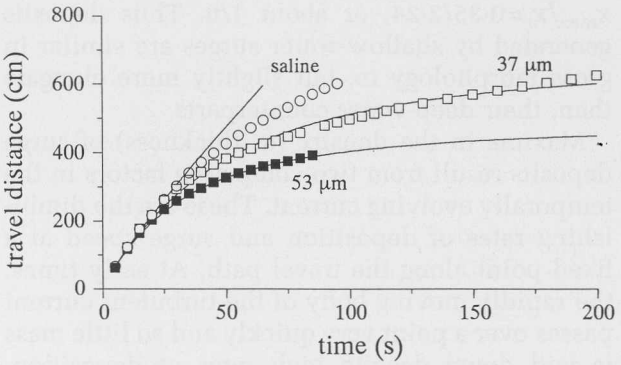

Fig. 2. Travel distance as a function of time for slumping gravity surges generated by the release of either a suspension of fine particles or a saline solution into a tank of fresh water. The initial reduced gravity for all currents was 22·9 cm s^{-2}. The equivalent diameters of the suspended particles are indicated in the figure. The symbols represent experimental observations of Bonnecaze *et al.* (1993) and the solid lines represent corresponding shallow-water, box-model predictions for the parameters listed in Table 1. The poor agreement at large times between the predictions and experimental observations for the shallow-water saline current is due to the onset of viscous effects (cf. Fig. 3) and deep-water conditions (cf. Fig. 4).

Table 1. Parameters for laboratory experiments and box-model predictions of the slumping of particle-driven gravity currents: lock volume, 0·30 m high × 0·26 m wide × 0·15 m long; $h_0=d=0·3$ m; $\rho_p=3217$ kg m^{-3}; $\rho_a=1000$ kg m^{-3}; $\nu=1·1\times10^{-6}$ m^2 s^{-1}.

Particle size (μm)	Initial excess mass (kg)	Re_0 ($\times10^4$)	β	c_s
Effects of particle size (Figs 2–4)				
37	0·4	14·3	0·0057	1·7
53	0·4	14·3	0·012	1·7
saline	0·4	14·3	0	1·0
Effects of initial bouyancy (Figs 5–7)				
37	0·1	6·7	0·011	2·0
37	0·2	9·4	0·0081	2·0
37	0·4	13·4	0·0057	1·7
37	0·8	18·9	0·0040	1·5
Areal density of final deposit (Fig. 8)				
23	0·1	6·7	0·044	1·3
53	0·1	6·7	0·024	1·7
23	0·4	13·4	0·0023	1·2
37	0·4	13·4	0·0057	1·7
53	0·4	13·4	0·012	1·7

populations having average diameters between 9 μm and 53 μm. Each experimental gravity current consisted of a relatively monodisperse suspension of particles. The total mass of solids ranged between 0·1 kg and 0·8 kg, with φ_0 less than 0·03 for all runs. These conditions are consistent with the assumptions of both their more complete model and with those of the box model described above. Further details of the BHL experiments are presented in the original study.

These carefully collected data provide a valuable basis for model verification. We show in Fig. 2, for example, measurements of the frontal travel distances as functions of time for gravity currents of suspended solids with the same initial buoyancy but varying particle size. Shown too are observations of an analogous saline current for comparison. Also presented in Fig. 2 are curves for the corresponding box-model predictions for shallow-water currents with the parameters given in Table 1. Only those data for suspension-driven currents that maintained a current-averaged Reynolds number, $(u_N h/\nu)(h/X_N)$, in excess of 2·25 were selected from the individual experiments reported by BHL, as is shown in the calculations of Fig. 3. Under these conditions, as discussed in BHL, gravity surges are considered to be relatively free of viscous effects. Note that the saline current is subject to viscous effects at times in excess of

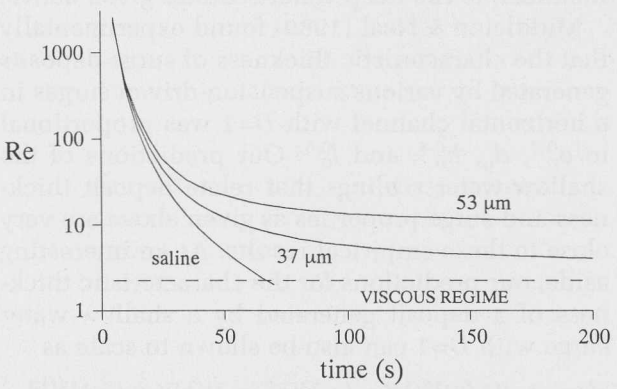

Fig. 3. Reynolds number, *Re*, as a function of time for the box-model gravity surges shown in Fig. 2 and for the parameters summarized in Table 1. The dashed line indicates the proposed critical value of 2·25 above which a balance between inertial and buoyancy dominates flow dynamics, and below which viscous effects become important.

about 50 s. Box-model currents for suspensions of 37 μm and 53 μm particles maintained a thickness in excess of $0·075d$, as shown in Fig. 4, which indicates that shallow-water conditions and slumping behaviour prevailed over the duration of those experiments. This is not the case for the saline current, which achieved deep-water conditions after about 40 s. Thus the combined effects of low Reynolds number and deep-water

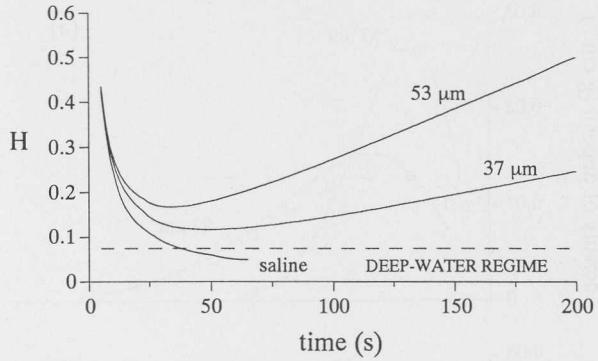

Fig. 4. The relative current thickness, $H=h/h_0$, as a function of time for the box-model gravity surges shown in Fig. 2 and for the parameters summarized in Table 1. The dashed line indicates the relative current thickness above which currents are in the shallow-water slumping regime.

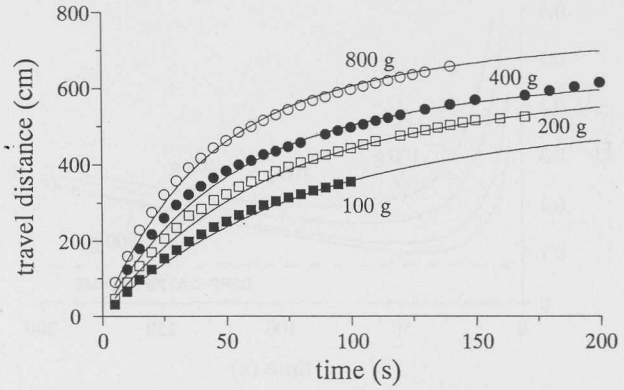

Fig. 5. Travel distance as a function of time for slumping gravity surges generated by the release of different suspensions of 37 μm diameter particles into a tank of fresh water. The initial particle masses for each current are indicated in the figure. Symbols represent experimental observations of BHL, and solid lines represent corresponding box-model predictions for the parameters listed in Table 1.

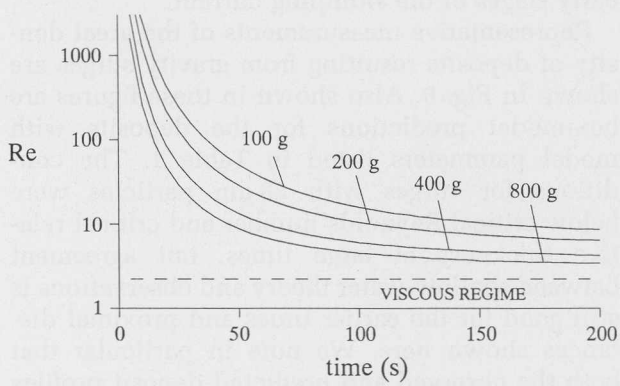

Fig. 6. Reynolds number, *Re*, as a function of time for the box-model gravity surges shown in Fig. 5 and the parameters summarized in Table 1. The dashed line indicates the proposed critical value of 2·25 above which a balance between inertial and buoyancy dominates flow dynamics, and below which viscous effects become important.

conditions rendered the experimental saline current unfit for comparison with the predictions from the shallow-water model at times in excess of about 50 s.

The box-model approximations described in Figs 2–4 capture the essential features of gravity-sure motion. Immediately following release, the intitially stationary volume collapses and approaches the self-similar behaviour of compositionally driven surges described by Eq. (13). In the shallow-water experiments, slumping-current behaviour is reflected in the nearly linear increase in length with time (cf. Huppert & Simpson, 1980). This stage is followed by a regime in which flow within the gravity surge gives rise to a gradual thickening with time. The current then continues to propagate as a decelerating, bore-like cloud of suspended particles. The loss of excess density through gravitational settling results in the loss of surge momentum and reduced speed as a function of time. The rates of density loss and flow dissipation through deposition increase with particle size. We note, too, from Fig. 4 that the box model indicates that onset and subsequent rates of current thickening are earlier and greater with increasing particle size.

Travel distances as functions of time for gravity currents with constant particle size and a range of initial particle concentrations are shown in Fig. 5. Also shown are our corresponding box-model predictions for shallow-water conditions with parameters given in Table 1. The initial concentrations are large enough to generate current velocities that maintain an inertia-buoyancy balance throughout the duration of each run; viscous effects are thus negligible, as indicated by the calculations shown in Fig. 6. The corresponding model currents maintained a thickness in excess of $0{\cdot}075d$, as shown in Fig. 7, indicating that shallow-water conditions and slumping behaviour again prevailed over the duration of each experimental current. We note, however, that in currents of a given particle size, the box model, in agreement with the full numerical model, indicates that the rates of reduction both of Reynolds numbers and of thickness of gravity currents are greater with increasing initial solids concentration. With increasing particle loading, the driving buoyancy is greater and thus rates of thinning

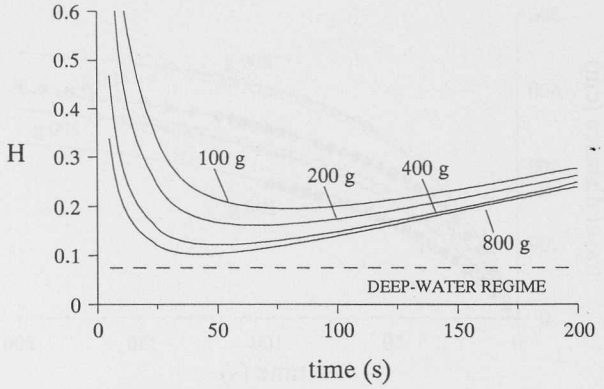

Fig. 7. The relative current thickness, $H=h/h_0$, as a function of time for box model gravity surges shown in Fig. 5 and for the parameters summarized in Table 1. The dashed line indicates relative current thickness above which the surges are in the shallow-water slumping regime.

due to current run-out are enhanced during the early stages of the slumping current.

Representative measurements of the areal density of deposits resulting from gravity surges are shown in Fig. 8. Also shown in these figures are box-model predictions for the deposits with model parameters listed in Table 1. The conditions for surges with 23 μm particles were below critical Reynolds number and critical relative thickness at large times, but agreement between shallow-water theory and observations is still good for the earlier times and proximal distances shown here. We note in particular that both the observed and predicted deposit profiles exhibit maxima at approximately 1 m downstream from the origin, with the displacement of the density maxima increasing with diminishing particle size. These features agree with predictions from Eq. (31). Sedimentation from a tail region that trails the main body of the current, which is not considered in the box model, contributes to the significant non-zero density of deposit near the origin of the current.

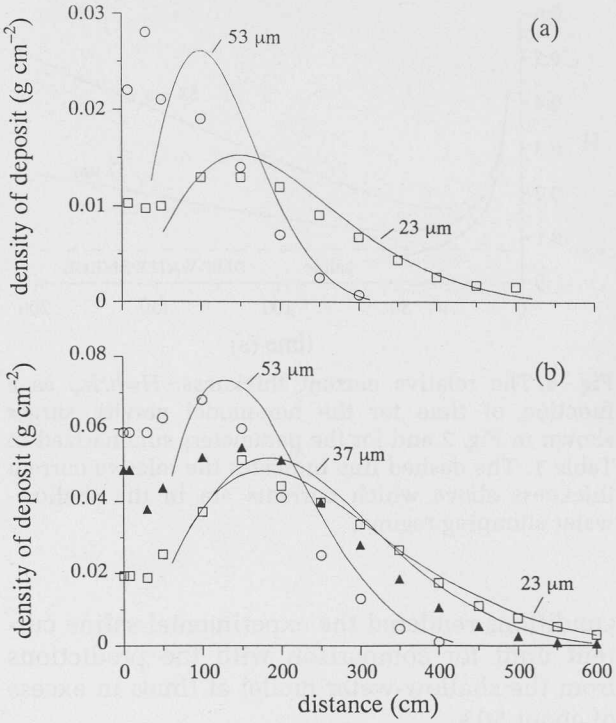

Fig. 8. The areal density of the final deposit as a function of distance along the travel path for gravity surges generated by the release of a fine-particle suspension into a tank of fresh water. The initial particle mass in the 0·30 m high × 0·26 m wide × 0·15 m long lock volume was 100 g and 400 g for the flows which generated the deposits shown in (a) and (b), respectively. Diameters of the particles in suspension are indicated in the figure. Symbols represent experimental observations of Bonnecaze *et al.* (1993), and the solid lines represent box-model predictions for the parameters listed in Table 1.

THE EFFECTS OF MORE THAN ONE PARTICLE SIZE

Our analysis to this point has been based on the premise that the size and the settling velocity of the particles in suspension are each well characterized by a single, central value. This approach is necessary to delineate properly the effects of particle size, but clearly limits the analogy with many natural phenomena. Given the success of our approximate model in describing the evolution of monodisperse suspensions, we consider here the large-time behaviour of a box model for a surge driven by a suspension of two distinct grain sizes. The description of the behaviour of polydisperse suspensions becomes unwieldy when more realistic, continuous distributions of particle sizes are considered, but we propose that an analysis accommodating this next level of complexity would yield results that are qualitatively similar to those summarized below. We focus on the asymptotic behaviour of the deep-water model but similar results can be obtained readily for shallow-water conditions as well.

In the case of a bidisperse suspension the settling law of Eq. (6) can be partitioned into the two expressions

$$\frac{\mathrm{d}\varphi_c}{\mathrm{d}t} = -\frac{w_{sc}\varphi_c}{h} \qquad (32a)$$

and

$$\frac{d\varphi_f}{dt} = -\frac{w_{sf}\varphi_f}{h} \qquad (32b)$$

where here and below the subscripts f and c denote the fine and coarse fractions, respectively. Dividing Eq. (32a) by Eq. (32b) and integrating the result, we relate the concentrations of the two size fractions by

$$\Phi_c = \Phi_f^{\gamma}, \qquad (33)$$

where the upper case symbols indicate the quantities relative to the initial values of each fraction and $\gamma=\beta_c/\beta_f$. The non-dimensional total concentration of solids is then given by

$$\Phi = \frac{\varphi_{co}}{\varphi_0}\Phi_c + \frac{\varphi_{f0}}{\varphi_0}\Phi_f.$$

Equation (11) for the thickness of currents in deep water can be cast into the form

$$H \approx \lambda_1 \Phi^{-1/3} T^{-2/3}, \qquad (34a)$$

where the initial geometry of the surge is incorporated into the coefficient λ_1. On the assumptions that $\beta_c \gg \beta_f$, that is, that the coarse and fine particles are well separated in size, and that φ_{co} be not too much larger than φ_{f0}, we find that $\Phi \approx \varphi_{f0}\Phi_f/\varphi_0$ and that

$$H \approx \lambda_1(\varphi_{f0}/\varphi_0)^{-1/3}\Phi_f^{-1/3}T^{-2/3}. \qquad (34b)$$

Substituting Eq. (34b) into the dimensionless version of Eq. (32b), and integrating the result for large time, we obtain an approximate solution for the concentration of the fine fraction given by

$$\Phi_f \approx \lambda_2 \beta_f^{-3} T^{-5} \qquad (T \gg 1), \qquad (35)$$

where

$$\lambda_2 \approx (5\lambda_1)^3 \varphi_0/\varphi_{f0}.$$

Because these results reflect large-time asymptotic behaviour, they do not necessarily match the initial conditions. A comparison of Eqs (34b) and (35) with Eqs (11) and (9) at large times implies that the large time evolution of the current and of the fine-fraction concentration does not depend on the presence of the coarse fraction. The large time evolution of the coarse fraction and its contribution to the surge deposit reflect the presence of the fine fraction, however, as we now show.

By analogy with Eq. (26), we see that the contribution of the coarse fraction η_c to the density of the deposit is given approximately by

$$\eta_c \approx (\varphi_{co}/\varphi_0)\beta_c T \Phi_c. \qquad (36a)$$

Using the approximation of Eq. (35) and the relationship defined in Eq. (33), we then find that Eq. (36a) indicates that the large time evolution of η_c is given approximately by

$$\eta_c \approx \lambda_3 \beta_c^{1-3\gamma} T^{1-5\gamma}, \qquad (36b)$$

where

$$\lambda_3 \approx [\lambda_2(\gamma)^3]^{\gamma}(\varphi_{co}/\varphi_0).$$

In the case of a single grain size, $\beta_c=\beta_f=\beta$, $\gamma=1$, $\Phi_c=\Phi_f=\Phi$ and thus $\eta \approx (5\lambda_1)^3\beta^{-2}T^{-4}$. In the case of the bidisperse suspension in which $\beta_f \ll \beta_c$, however, the quantity $5\gamma-1$ in the exponent of the power law relating η_c and T in Eq. (36b) is much greater than 4, the value associated with the single grain-size case. The implication is that the rate of decrease of the concentration of the coarse fraction is enhanced from what it would be if no fine material were present. As a result, the contribution of the coarse fraction to the deposit diminishes at a much greater rate than if no fine material were present. The magnitude of this effect is dependent on the ratios of the settling velocities and of the initial concentrations of the respective size fractions.

The physical mechanism responsible for this behaviour is the greater degree of surge thinning, and thus an enhanced deposition rate of the coarse fraction, due to the relatively rapid run-out of the surge driven by the longer lived fine-grain component of the suspension. We conclude that whereas coarse material may be carried further than if there were no fine material present, there is nevertheless a very strong potential for size grading, which occurs as a function of time during the formation of distal deposits by turbidity surges. If there is sufficient material in the driving suspension for continued propagation of the surge at large times, this grading appears in space. If the late-stage surge is moving only very slowly, however, then the sorting of grain sizes manifests itself in a deposit that is vertically graded. The extent of the sorting along either the horizontal or vertical axis is dependent on the exact ratios of the settling velocities and the initial concentrations of the respective size fractions. These interpretations are consistent with the observations of Middleton (1967) and Middleton & Neal (1989) regarding the segregation of grain sizes in deposits generated by lock-release suspensions of varying degree of initial sorting. Thus Eq. (36) provides the basis for a possible explanation of sorting in distal deposits generated by turbidity currents on surfaces that are horizontal or nearly so.

DISCUSSION

We have developed a box model that approximates the propagation of and the deposition from a two-dimensional, particle-driven gravity surge as it travels across a horizontal surface following release from a lock. The approach is based on a small perturbation to the scaling relationships for the thickness of analogous, compositionally driven flows in which inertia and buoyancy are in appropriate balance. This modification leads to a description of the evolution of particle concentration due to gravitational settling, and this result, coupled with the modified scaling for surge thickness, is then used to re-estimate the front velocity and travel distance of the dissipating current as functions of time. The distribution of particle deposits laid down by the surge is related to the change in particle concentration that occurs as the surge moves over a fixed point.

The agreement between the predictions of our analytical model and the experimental observations reported by Bonnecaze *et al.* (1993) for suspension-driven surges in a shallow-water flume is good. Box-model predictions for the scaling relationships between the characteristic thickness of a deposit and the initial solids concentration, diameter of particles in suspension, and geometry of a surge also agree well with the power-law relationships determined experimentally by Middleton & Neal (1989). Although this agreement is achieved with the introduction of an adjustable coefficient, we hasten to point out that this coefficient is determined experimentally to be near unity and to vary only by about $\pm 25\%$ ($1{\cdot}6 \pm 0{\cdot}4$) over (at least) a twofold range of particle diameters, an eightfold range in initial solids concentration of suspensions, and a sixfold range of the critical model parameter β without any discernible trends in our experiments. As β tends to zero, however, the values of the coefficients c_d and c_s introduced in the respective analyses for deep- and shallow-water flows must, by their definition, approach unity.

The validation provided by the comparison of the model and experimental results thus clearly suggests that the box model describes the essential behaviour of slumping, particle-driven gravity surges observed on experimental time-scales. The need to adjust the coefficient c_d is expected to be considerably less under deep-water conditions of natural settings than was required of c_s for shallow-water flows generated in the laboratory. This is so for two reasons. The critical model parameter β, which provides a measure of the settling velocity of fine-grain, suspended particles, is expected to be considerably less than the values characterizing most laboratory experiments. In addition, the coefficient c_s essentially provides a trailing boundary condition that is strongly affected by the return flow that results from overall continuity in the shallow-water flumes. This effect is non-existent in deep-water flows. For useful estimates pertaining to deep-water flows we therefore propose that the coefficient c_d be set to unity for approximations of the dimensionless frontal speed (Eq. 12), frontal travel distance (Eq. 13), and distribution of particle deposits (Eqs 13 and 25). We demonstrate the potential usefulness of these approximations at the end of our discussion.

There are several deficiencies in the box-model approach. The two-dimensional gravity current is assumed to be inviscid and to collapse in a series of equal-area rectangles. The frontal velocity of the unsteady current is defined by a steady-state Froude number. The entrainment of ambient fluid and friction are not considered explicitly, and re-entrainment of deposited particles on the bed is not considered at all. Finally, the scaling for the current thickness is based initially on instantaneous values of particle concentration and position of the current tail. Although these arguments are reasonable for a slowly varying current, accumulated error due to the history of changes in particle concentration and position of the tail over the life of a gravity current may ultimately invalidate box-model predictions at very large times. Under these far-field conditions, however, the behaviour of a suspension-driven surge may be better considered in terms of a fully developed, fluid-entraining flow (Hallworth *et al.*, 1993; Dade *et al.*, 1994). The behaviour of the box-model equations for slumping currents is nevertheless enlightening, as we demonstrated in obtaining several scaling relationships between surge characteristics and deposit geometry and in an analysis of the evolution of suspensions characterized by two particle sizes.

Thickening of gravity currents with time

At first glance it is not clear why this box model, or the more complete numerical analysis of BHL, should be accurate when entrainment of ambient fluid is explicitly neglected. Hallworth *et al.* (1993) reported that turbulent, saline gravity surges propagating across horizontal surfaces in the laboratory are subject to significant rates of entrainment of ambient fluid and even higher

fluxes of dense solution to a quasi-stagnant tail. These processes occur at travel distances in excess of the slumping distance $q_0/(0{\cdot}075d)$, however, which corresponds to the point in time at which the initially shallow-water currents begin to exhibit self-similar behaviour resulting from an exclusive balance between buoyant and inertial forces. According to Hallworth *et al.*, no measureable exchange of surge and ambient fluid occurs in the head while a gravity current is in the slumping regime. The reduced rates of thinning due to surge run-out followed by gradual thickening of particle-driven gravity currents shown in Figs 4 and 7 suggest that some particle-driven surges generated in the laboratory may stay in the slumping phase for longer times and thus exhibit little or no exchange with the ambient fluid.

The thickening behaviour of a suspension-driven surge is quite different from that of a compositionally driven current, and we interpret it to reflect local conservation of the pressure gradient existing at the surge head. With the loss of excess buoyancy through gravitational settling of suspended particles, the driving pressure gradient at the head is conserved locally by arrival of faster-moving fluid from behind. Alternatively, this phenomenon may be thought to reflect the conservation of total energy of the current through gains in potential energy via thickening to offset losses in kinetic energy due to deposition. When coupled with the conservation of volume, flow convergence near the head results in the thickening of a surge and the development of a bore-like flow.

A related consequence of surge thickening is the preservation of inertial conditions in suspension-driven currents for periods longer than expected for analogous saline flows. Huppert & Simpson (1980) showed that the dimensionless time of transition from inertia-dominated to viscous-dominated regimes in a saline current is given by

$$T_c = KQ_0Re_0^{3/7} = KQ_0^{4/7}\,(g'_0h_0^3/\nu^2)^{3/14} \qquad (37)$$

in terms of the initial value of the Reynolds number of the current $Re_0=(u_Nh/\nu)(h/X_N)$ evaluated at $T=1$, where K was determined experimentally to be approximately 0·5. Onset of thickening of a shallow-water surge due to particle deposition, on the other hand, occurs when $dH/dT=0$, which can be applied to Eq. (18) to yield an estimate of the dimensionless time T_β given by

$$T_\beta \approx 0{\cdot}92\sigma_s^{-7/13} \approx 2{\cdot}6D^{-2/13}(c_s/\beta)^{7/13}Q_0^{6/13}. \qquad (38)$$

At times in considerable excess of T_β the relative thickness of the surge grows asymptotically as βT. If $T_\beta<T_c$ a particle-driven surge will begin to thicken before reaching the point at which the flow begins to exhibit subcritical Reynolds numbers. Inasmuch as the relevant Reynolds number is proportional to some power of the surge height, a suspension-driven current for which $T_\beta<T_c$ maintains sufficiently high Reynolds numbers to remain inertial for much longer period than will an analogous, compositionally driven current. Upon rearrangement, Eqs (37) and (38) yield the condition

$$\beta>5{\cdot}9c_sK^{-13/7}D^{-2/7}Q_0^{-1}Re_0^{-39/49} \qquad (39)$$

that must be met to ensure that this effect indeed takes place. For the experimental conditions considered here and summarized in Table 1, thickening of surges begins before onset of low Reynolds number conditions due to thinning when particle diameters are 30–40 μm or larger (cf. Figs 3 and 6). Ironically, the larger the particle size suspended in a current with given initial conditions, the longer the current will travel in an inertial regime even though it is rapidly dissipating due to a greater rate of deposition.

By similar arguments, we find that the suspension-driven current released in shallow water begins to thicken before running out to the point at which $h\leq 0{\cdot}075d$ if

$$\beta>0{\cdot}008c_sQ_0D^{5/2}. \qquad (40)$$

For the experimental conditions considered here, a surge remains a shallow-water current if the diameters of the particles in suspension are 30–40 μm or larger (cf. Figs 4 and 7). Equations (39) and (40) are useful guidelines for the design of lock-release experiments in horizontal channels providing analogues for inertial turbidity currents.

Application to the geological record

Box models describing suspension-driven gravity currents provide exciting opportunities for the analysis of the dynamics and deposits of natural phenomena. Downstream thinning and fining of gravity-surge deposits are essential features of our model and correspond to observations of many naturally occurring surge deposits called turbidities (Walker, 1967). More precise application of box models to geophysical gravity currents must nevertheless await further study of the effects of topography, entrainment of ambient fluid or bed sediment, and very dense concentrations of

Table 2. Length- and time-scales for the analysis of a deposit generated by a non-entraining surge.†

	Deep-water surge	Shallow-water surge
	$h/d \leq 0{\cdot}075$	$h/d > 0{\cdot}075$
Length-scales		
Maximum deposit thickness, τ_{max}	$(\varphi_0/\varphi_b)(q_0^2 w_s^2/g_0')^{1/5}$	$1{\cdot}3\, D^{-2/13}(\varphi_0/\varphi_b)(q_0^6/h_0^2 w_s^6 g_0'^3)^{1/13}$
Characteristic deposit thickness, $(\varphi_0/\varphi_b)(q_0/x_r)$	$\tau_{max}/3$	$\tau_{max}/3$
Distance from the origin:		
to distal end of deposit, x_r	$3\,(g_0' q_0^3/w_s^2)^{1/5}$	$2{\cdot}2\, D^{2/13}\,(g_0'^3 q_0^7 h_0^2/w_s^6)^{1/13}$
to maximal thickness, x_{max}	$x_r/5$	$x_r/6$
Times-scales		
Time required for the surge centre to reach x_{max}	$0{\cdot}7\,(q_0^2/g_0' w_s^3)^{1/5}$	$1{\cdot}1\, D^{-2/13}\,(q_0^6/h_0^2 g_0'^3 w_s^7)^{1/13}$
Time required for the surge to reach x_r	$t \gg 2\,(q_0^2/g_0' w_s^3)^{1/5}$	$t \gg 3\, D^{-2/13}\,(q_0^6/h_0^2 g_0'^3 w_s^7)^{1/13}$

†These are scaling arguments only: the coefficients reflect the behaviour of a surge driven by a fine-grain suspension and described by our box model in which the value of the ratio $w_s/(g_0' h_0)^{1/2}$ is small. A surge is assumed to be a flow of high Reynolds number during its entire history.
φ_0 is the initial concentration of solids suspended in the surge; φ_b is the concentration of solids in the bed; g_0' is the reduced gravity of the initial suspension; q_0 is the initial volume per unit width of the surge; h_0 is the initial height of the surge; D is the ratio of the ambient depth d to h_0; w_s is the average settling velocity of the fine particles in suspension.

suspended sediment. We plan to address aspects of these problems in the future.

Froude-number conditions at the turbulent current head are unlikely to be a strong function of slope (Hopfinger, 1983), and our present box model becomes broadly applicable if we limit our discussion to non-eroding turbidity currents on low-angle slopes for which the flow is two-dimensional and the dissipation due to entrainment of ambient fluid is secondary to the effects of particle deposition. Under these conditions, the notion of a critical Reynolds number for the onset of viscous or rheological damping of thinning gravity currents is consistent with observations and ideas described by McCave & Jones (1988) regarding the rapid emplacement of homogeneous muds in some deep-sea turbidities. If very dense, cohesive suspensions are involved, as proposed by McCave & Jones, the following must be considered. Firstly, the particle settling velocity would be reduced dramatically (resulting in behaviour that is more like rapidly thinning saline currents; cf. Figs 3 and 4). Secondly, the large initial buoyancy would ensure relatively rapid run-out (cf. Figs 6 and 7). Finally, the enhanced viscosity of the dense suspensions may include both Newtonian and non-Newtonian effects. Each of these factors contributes to the damping of an inertial gravity current and the rapid emplacement of the sediment load.

Our analysis also suggests that under some conditions the overall thickness of proximal deposits resulting from particle-driven gravity surges should exhibit a maximum at a predictable distance downstream from the source. As a result, turbidities resulting from supension-driven surges debouching on flat, basin plains should be lenticular bodies with basal coarse layers exhibiting upstream maximal thickness and finer layers exhibiting downstream maxima. Such deposit geometries have indeed been observed in calcareous turbidities with overall lengths of 15–25 km laid down in ancient, near-reef basins (Meischner, 1964).

A lenticular geometry for the surge deposit is also observed in the 'Black Shell turbidite' of Pleistocene age and extending at least 500 km across the relatively flat and featureless Hatteras Abyssal Plain. The deposit achieves a maximum overall thickness of several metres at a distance approximately 200 km downstream from the inferred point of entry on to the deep-sea plain, with longitudinal (as well as lateral) displacement of maximum deposition of basal fine sands and overlying silt- and clay-rich muds (Elmore *et al.*, 1979). The width of the surge deposit is about 100–200 km and is clearly two-dimensional, suggesting that the flow of origin was also two-dimensional.

In Table 2 we summarize the scaling arguments that have emerged from our analytical box model for small $\beta = w_s/(g_0' h_0)^{1/2}$. We note from Eq. (28), for example, that the maximum thickness of a surge deposit should be about $(\varphi_0/\varphi_b)(w_s^2 q_0^2/g_0')^{1/5}$

(where $\varphi_b \approx 0{\cdot}5$ is the concentration of particles in the bed) and should occur at a distance downstream from the finite-volume source that is given approximately by $0{\cdot}6(g'_0 q_0^3/w_s^2)^{1/5}$. From Eq. (14b) we expect that the surge deposit should essentially vanish at downstream distances exceeding $3(g'_0 q_0^3/w_s^2)^{1/5}$ for which the surge took a period of time in excess of $2(q_0^2/g'_0 w_s^3)^{1/5}$ to traverse.

We can suggest therefore, in terms of these scalings, that one likely event leading to the formation of the Blackshell turbidite is a surge with an initial height $h_0 \approx 500$ m, initial length $l_0 \approx 10$ km, and an initial volumetric concentration $\varphi_0 \approx 0{\cdot}05$ of suspended particles that are, on average, 20 μm in diameter and of the same density as quartz. (The term 'initial' refers to the state of the surge upon entry into the deep-sea basin, and not necesarily at the upslope point of current origin due to the catastrophic failure of the sea-floor.) The value of the critical model parameter β is of the order 10^{-5} and so our scaling arguments are indeed applicable. Such a flow would have generated a deposit with a maximal thickness of about 2 m at a distance of 150 km from the point of entry on to the abyssal plain. The overall length of the deposit would be in excess of 700 km, and the surge would have traversed and laid down the deposit over this run-out distance during a period of a few days. We expect bedforms within the deposit to reflect the changing sediment concentration and propagation speed. Bedforms should thus evolve from those due to high rates of fallout of the suspended load and high flow intensities in the proximal region to those due to relatively lower rates of fallout and lower flow intensities in the distal region (cf. Lowe, 1988). From our analysis of the effects of more than one grain size we expect that the grain size of the deposit should diminish and that the degree of sorting, either in the vertical or in the horizontal, should increase in the downstream direction. These notions are in agreement with the observations reported by Elmore *et al.* (1979). There are, of course, other combinations of surge properties that could have produced a similar gross morphology, but our description seems a likely scenario given the constraint of the grain size and overall geometry of the silty mud deposit.

We are moving steadily toward more complete descriptions of the gravity currents that generate turbidities. The challenge then remaining will be to reconstruct with confidence the flows that shaped these interesting and economically important features of the geological record.

ACKNOWLEDGMENTS

We thank R. T. Bonnecaze, R. C. Kerr, J. R. Lister, G. V. Middleton, J. T. Smith and J. S. Turner for their reviews of earlier versions of the text. Discussions with G. I. Barenblatt and A. W. Woods also contributed to our understanding of gravity currents. This research was supported by the NERC.

REFERENCES

Allen, J.R.L. (1984) *Sedimentary Structures. Developments in Sedimentology,* **30,** Elsevier, New York, 2 vols.

Bonnecaze, R.T., Huppert, H.E. and Lister, J.R. (1993) Particle-driven gravity currents. *J. Fluid Mech.,* **250,** 339–369.

Dade, W.B., Lister, J.R. and Huppert, H.E. (1994) Fine-sediment deposition from gravity surges on uniform slopes. *J. Sediment. Petrol.,* **A64,** 423–432.

Elmore, R.D., Pilkey, O.H., Cleary, W.J. and Curran, H.A. (1979) Black Shell turbidite, Hatteras Abyssal Plain, western Atlantic Ocean. *Geol. Soc. Am. Bull.,* **90,** 1165–1176.

Gradshteyn, I.S. and Ryzhik, I.M. (1980) *Tables of Integrals, Series, and Products.* Academic Press, London, 1160pp.

Hallworth, M.A., Phillips, J.C., Huppert, H.E. and Sparks, R.S.J. (1993) Entrainment in turbulent gravity currents. *Nature,* **362,** 829–831.

Hopfinger, E.J. (1983) Snow avalanche motion and related phenomena. *Ann. Rev. Fluid Mech.,* **15,** 47–76.

Huppert, H.E. and Simpson, J.E. (1980) The slumping of gravity currents. *J. Fluid Mech.,* **99,** 785–799.

Lowe, D.R. (1988) Suspended-load fallout rate as an independent variable in the analysis of current structures. *Sedimentology,* **35,** 765–776.

Martin, D. and Nokes, R. (1988) Crystal settling in a vigorously convecting magma chamber. *Nature,* **332,** 534–536.

McCave, I.N. and Jones, K.P.N. (1988) Deposition of ungraded muds from high-density non-turbulent turbidity currents. *Nature,* **333,** 250–252.

Meischner, K.-D. (1964) Allodapische kalke, turbidite in riff-nahen sedimentations-becken (Allodapic limestones, turbidites in near reef sedimentary basins). In: *Turbidites. Developments in Sedimentology,* **3,** pp. 156–191. (Ed. by A. H. Bouma and A. Brouwer), Elsevier, Amsterdam.

Middleton, G.V. (1966a) Experiments on density and turbidity currents I. Motion of the head. *Can. J. Earth Sci.,* **3,** 523–546.

Middleton, G.V. (1966b) Experiments on density and turbidity currents. II. Uniform flow of density currents. *Can J. Earth Sci.,* **3,** 627–636.

Middleton, G.V. (1967) Experiments on density and turbidity currents III. Deposition of sediment. *Can. J. Earth Sci.,* **4,** 475–505.

Middleton, G.V. (1993) Sediment deposition from turbidity currents. *Ann. Rev. Earth Planet. Sci.*, **21**, 89–114.

Middleton, G.V. and Neal, W.J. (1989) Experiments on the thickness of beds deposited by turbidity currents. *J. Sediment. Petrol.*, **59**, 297–307.

Riddell, J.F. (1969) A laboratory study of suspension-effect density currents. *Can. J. Earth Sci.*, **6**, 231–246.

Simpson, J.E. (1982) Gravity currents in the laboratory, atmosphere, and ocean. *Ann. Rev. Fluid Mech.*, **14**, 213–234.

Simpson, J.E. (1987) *Gravity Currents in the Atmosphere and the Laboratory.* Halstead Press.

Walker, R.G. (1967) Turbidite sedimentary structures and their relationship to proximal and distal depositional environments. *J. Sediment. Petrol.*, **37**, 25–43.

Manuscript received 18 November 1993; revision accepted 19 July 1994

APPENDIX A

Derivation of the scaling equations for the height of a gravity surge

Here we derive the main relationships needed to obtain Eqs (5b) and (15b).

Gravity surges in deep-water surroundings

From Eqs (1) and (3b) we note that

$$u_N = \dot{x}_N = 1{\cdot}19(g'h)^{1/2}. \quad \text{(A1)}$$

Using Eqs (2) and (4) we can re-express Eq. (A1) as

$$\dot{x}_N = 1{\cdot}19(g'_0 q_0)^{1/2}(\varphi/\varphi_0)^{1/2} a^{-1/2} x_N^{-1/2}, \quad \text{(A2)}$$

where

$$a = 1 - x_T/x_N. \quad \text{(A3)}$$

Note that a is only slightly less than unity if the trailing boundary lags the leading edge by a considerable distance. Integrating Eq. (A2), we see that one of the solutions is

$$x_N = 1{\cdot}47(g'_0 q_0)^{1/3}(\varphi/\varphi_0)^{1/3} t^{2/3} \varphi^{-1/3} \langle(\varphi/a)^{1/2}\rangle^{2/3}, \quad \text{(A4)}$$

where the angle brackets on the right-hand side of Eq. (A4) indicate a temporally averaged quantity. Equation (A4) corresponds to the expression for the self-similar length of a buoyancy-conserving surge in deep water as a function of time, expressed in a form that allows for the slow loss of particles due to settling. Substitution of Eq. (A4) into Eq. (4) yields the estimate for h, in agreement with Eq. (5b), given by

$$h = 0{\cdot}68 c_d (q_0^2/g'_0)^{1/3}(\varphi/\varphi_0)^{-1/3} t^{-2/3}, \quad \text{(A5a)}$$

where

$$c_d = \left(\frac{\varphi^{1/2}}{a^{3/2}\langle(\varphi/a)^{1/2}\rangle} \right)^{2/3}. \quad \text{(A5b)}$$

Incorporated in the coefficient c_d are the histories of both the driving buoyancy and the motion of the current tail. Our treatment of c_d as a constant reflects the assumptions that a suspension-driven surge is slowly varying and that for the bulk of the flow history the tail lags behind the current head by a considerable distance. Thus the quantity that has been averaged over time can be approximated by instantaneous values and $c_d \approx a^{-2/3} \approx 1$, which suggests that the slow variation in a during the life of a deep-water surge will affect the value of c_d only weakly. The calculation of the frontal travel distance x_N as a function of time is achieved by the integration of a modified form of u_N over time rather than direct substitution into Eq. (A4). This step ensures that c_d is indeed nearly constant (due to successive integral averaging) and results in the approximation of Eq. (13) for x_N that exhibits the asymptotic limit x_r, as discussed in the text.

Gravity surges in shallow-water surroundings

From Eqs (1) and (3a) we note that

$$u_N = \dot{x}_N = 1/2 d^{1/3} g'^{1/2} h^{1/6}. \quad \text{(A6)}$$

Using Eqs (2) and (4) we can re-express Eq. (A1) as

$$\dot{x}_N = 1/2 d^{1/3} g'^{1/2}_0 (\varphi/\varphi_0)^{1/2} q_0^{1/6} a^{-1/6} x_N^{1/6}. \quad \text{(A7)}$$

A solution to Eq. (A7) is

$$x_N = 0{\cdot}63(g'^3_0 d^2 q_0)^{1/7}(\varphi/\varphi_0)^{3/7} t^{6/7} \varphi^{-3/7} \langle \varphi^{1/2}/a^{1/6}\rangle^{6/7}. \quad \text{(A8)}$$

Substitution of Eq. (A8) into Eq. (4) yields an estimate for h, in agreement with Eq. (15b), given by

$$h = 1{\cdot}59 c_s (q_0^6/g'_0 d^2)^{1/7}(\varphi/\varphi_0)^{-3/7} t^{-6/7}, \quad \text{(A9a)}$$

where

$$c_s = \left(\frac{\varphi^{1/2}}{a^{7/6}\langle \varphi^{1/2}/a^{1/6}\rangle} \right)^{6/7}. \quad \text{(A9b)}$$

Our treatment of c_S as a constant in our box-model approximations has the same basis as our earlier treatment of c_d. Comparison of Eqs (A5b) and (A9b), however, suggest that whereas $c_d \approx a^{-2/3}$, $c_s \approx a^{-6/7}$. Thus the coefficient c_s for shallow-water flows is slightly more sensitive to a trailing boundary condition that is weakly unsteady than is the coefficient c_d for deep-water surges. As a result c_d will be further from unity

than c_d. The good comparison between laboratory data and the predictions of our box model with the assumption that the coefficient c_s is a constant gives us confidence that the model yields good estimates of the behaviour of a suspension-driven surge in a deep-water basin for which c_d is taken to be a constant very near unity. For surges driven by suspensions for which β tends to zero, c_d must by definition tend to 1.

APPENDIX B

Expressions for the propagation distance X_N

Here we present the complete expressions for $f_d(\sigma_d T)$ and $f_s(\sigma_s T)$ which appear in Eqs (13) and (20), respectively, and describe the propagation distance X_N as a function of time T. For deep-water surges, $f_d(\sigma_d T)$ is given by

$$f_d(\sigma_d T) = -0{\cdot}59 c_d^{1/2}\left[\ln[1+(\sigma_d T)^{1/3}] + \sum_{n=0}^{1}\cos\left\{\frac{(2n+1)2\pi}{5}\right\}\ln\left[1+(\sigma_d T)^{2/3}-2(\sigma_d T)^{1/3}\cos\left\{\frac{(2n+1)\pi}{5}\right\}\right] - 2\sum_{n=0}^{1}\sin\left\{\frac{(2n+1)2\pi}{5}\right\}\left(\arctan\left[\frac{(\sigma_d T)^{1/3}-\cos\left\{\frac{(2n+1)\pi}{5}\right\}}{\sin\left\{\frac{(2n+1)\pi}{5}\right\}}\right]-\frac{(4n-3)\pi}{10}\right)\right] \quad \text{(B1)}$$

For shallow-water flows, $f_s(\sigma_s T)$ is given by

$$f_s(\sigma_s T) \approx -0{\cdot}29 c_s^{1/6}\left[\ln[1+(\sigma_s T)^{1/7}] + \sum_{n=0}^{5}\cos\left\{\frac{(2n+1)6\pi}{13}\right\}\ln\left[1+(\sigma_s T)^{2/7}-2(\sigma_s T)^{1/7}\cos\left\{\frac{(2n+1)\pi}{13}\right\}\right] - 2\sum_{n=0}^{5}\sin\left\{\frac{(2n+1)6\pi}{13}\right\}\left(\arctan\left[\frac{(\sigma_s T)^{1/7}-\cos\left\{\frac{(2n+1)\pi}{13}\right\}}{\sin\left\{\frac{(2n+1)\pi}{13}\right\}}\right]-\frac{(4n-11)\pi}{26}\right)\right]. \quad \text{(B2)}$$